International Journal of Digital Earth

ISSN: 1753-8947 (Print) 1753-8955 (Online) Journal homepage: www.tandfonline.com/journals/tjde20

A spatial context-aware model for climate model data fusion

Jinyu Meng, Zengchuan Dong & Yongze Song

To cite this article: Jinyu Meng, Zengchuan Dong & Yongze Song (2025) A spatial context-aware model for climate model data fusion, International Journal of Digital Earth, 18:1, 2509099, DOI: 10.1080/17538947.2025.2509099

To link to this article: https://doi.org/10.1080/17538947.2025.2509099

Published online: 25 May 2025.

INTERNATIONAL JOURNAL OF DIGITAL EARTH
2025, VOL. 18, NO. 1, 2509099
https://doi.org/10.1080/17538947.2025.2509099

RESEARCH LETTER

OPEN ACCESS Check for updates

A spatial context-aware model for climate model data fusion

Jinyu Meng[a], Zengchuan Dong[a] and Yongze Song[b]

[a]College of Hydrology and Water Resources, Hohai University, Nanjing, People's Republic of China; [b]School of Design and the Built Environment, Curtin University, Perth, Australia

ABSTRACT

Acquiring more accurate climate model data is crucial for conducting precise regional climate studies. Most studies use linear weighting methods or a single machine learning model fusing multiple climate model datasets to reduce uncertainty. However, these methods use the identical model globally and ignore local characteristics of various climate models. This study develops a spatial context-aware fusion (SCAF) model to fuse multi-source climate data by constructing distinct models at different spatial locations, capturing local climate features and enhancing the regional applicability of the climate data. The developed SCAF model is implemented in the fusion of radiation data using 22 CMIP6 climate models in the upper Yellow River. Results show that SCAF can effectively fuse regional radiation data with correlation coefficients higher than 0.95 between the fused data and observed data at any location across space. As such, SCAF can effectively capture regional climate characteristics through spatially local modelling. In addition, the analysis of future radiation trends shows that the rate of radiation decline accelerates with stronger scenario models, with decreases ranging from 0.123 to 0.7771 W/m^2 per decade. The model demonstrates significant advantages and has a broad potential to effectively fuse regional climate models.

ARTICLE HISTORY
Received 17 October 2024
Accepted 5 May 2025

KEYWORDS
Spatial context-aware model; climate change; climate model data fusion; radiation

1. Introduction

Currently, climate change has become a research hotspot, and accurate climate data is the basis for conducting climate change research. The quality of climate data directly impacts climate research's scientific validity, reliability, and policy decisions (Deser et al. 2020; Petzold et al. 2020). Accurate data are essential for assessing climate change trends and provide a critical foundation for analysing complex changes in the climate system (Song et al. 2020). Accurate climate data also facilitate the development of precise climate prediction models, which enhance the simulation of future climate scenarios (Li et al. 2022). The current climate model data come from different research organisations, and there are large uncertainties in the climate data from a single source. At the

CONTACT Zengchuan Dong zcdong@hhu.edu.cn College of Hydrology and Water Resources, Hohai University, Nanjing, 210098, People's Republic of China

same time, the use of simple linear weighting or a single machine learning model for multi-model fusion also has many problems, such as the inability to fully consider the applicability of the model in different regions. Therefore, the use of context-aware models becomes an important way to solve the above problems.

Global climate models (GCMs), such as those used in the Coupled Model Intercomparison Program Phase 6 (CMIP6) (Tebaldi et al. 2021), are widely employed to predict future changes in renewable energy sources, including wind (Esnaola et al. 2024; Martinez and Iglesias 2022) and solar energy (Dutta, Chanda, and Maity 2022; Ferreira, Reboita, and Ribeiro 2024). These models provide substantial data support for assessing renewable energy sources and predicting the potential impacts of future climate change on energy production (Ha et al. 2023). However, uncertainties inherent in climate models, such as climate variability, limit the predictive capabilities of a single model.

Uncertainty in climate models comes from several sources, including model structure (Song, Shen, et al. 2021; Song, Thatcher, et al. 2021), parameter selection (Zelinka et al. 2020), parameterisation of physical processes, and initial condition setting. These uncertainties introduce stochasticity and potential bias to the prediction results of a single model (Aadhar and Mishra 2020; Hirsch et al. 2021). In addition, different climate models employ different technical approaches and assumptions in simulating the Earth's climate system, which gives each of them unique strengths and limitations that vary in accuracy and applicability.

Multi-model fusion is increasingly required to reduce the uncertainty in predictions as relying on a single model often find it difficult to fully reflect the complexity and diversity of the climate system. The existing approaches for the fusion of multiple climate model data can be classified into two categories. The first category is the linear weighting approaches, where multiple modal data are fused using a linear model, including difference weight ensemble (DWE) (Basak et al. 2023; Shuaifeng and Xiaodong 2022), multi-model ensemble (MME) (Dutta et al. 2022; Tian et al. 2021), and weighted multi-model ensemble (WMME) (Basak, Garlapati, and Patel 2024). In addition, with the rapid development of artificial intelligence, machine learning methods have been widely applied to the fusion of climate model data to address nonlinear problems. Typical techniques include random forests (RF) (Chen et al. 2024; Dey et al. 2022), support vector machines (SVM) (Kayhomayoon et al. 2023; Singh et al. 2023), and neural networks (NN) (Roshani and Hamidi 2022). Artificial intelligence-based nonlinear methods can effectively capture the nonlinear relationships between climate patterns, but current studies usually use a unified model to fuse the entire study area, ignoring the heterogeneous features that may exist in different spatial locations.

However, there are still critical challenges in the existing climate model data fusion approaches. First, the linear weighting approaches are difficult to effectively reflect the complex process of actual climate change, limiting their applications in dealing with sophisticated climate characteristics. Second, the current studies of machine learning-based climate model data fusion primarily rely on a single model or the fusion of different parameters from a single model across the entire area, often ignoring the local variability of meteorological data and thus failing to adequately characterise regional climate change (Song, Shen, et al. 2021; Song, Thatcher, et al. 2021).

This study develops a spatial context-aware fusion (SCAF) model to fuse multi-source climate data by constructing distinct models at different spatial locations, capturing local

climate features and enhancing the regional applicability of the climate data. SCAF performs perceptual learning and prediction by training different machine learning models at different spatial locations and adjusting their parameters accordingly. SCAF enhances the accuracy of data fusion and better reflects local climate change characteristics, improving the model's adaptability and expressiveness in addressing regional climate differences. The developed SCAF model is implemented in the fusion of radiation data using 22 CMIP6 climate models in the upper Yellow River.

2. Research data and methodology

2.1. Study area and observations

This study's area is Qinghai and Gansu provinces, located in the upper reaches of the Yellow River Basin (UYRB) (as shown in Figure 1). The Upper Yellow River Clean Energy Base (UYCEB) is in Qinghai Province, and the Hexi Corridor Clean Energy Base (HCCEB) is in Gansu Province. UYCEB and HCCEB are important components of China's nine planned clean energy bases. Qinghai and Gansu are located on high plateaus with high terrain. The study area is blessed with solar energy resources and rich decertified land resources with up to 2500–3650 h of sunshine throughout the year, making solar power an important form of energy in the area. Due to the sparse and uneven distribution of meteorological stations in the study area, this paper uses the ERA5 dataset for solar energy prediction studies in the UYRB, and the application of ERA5 radiation data has been widely verified in China (Deng et al. 2022; Jiang et al. 2021; Wang et al. 2023)

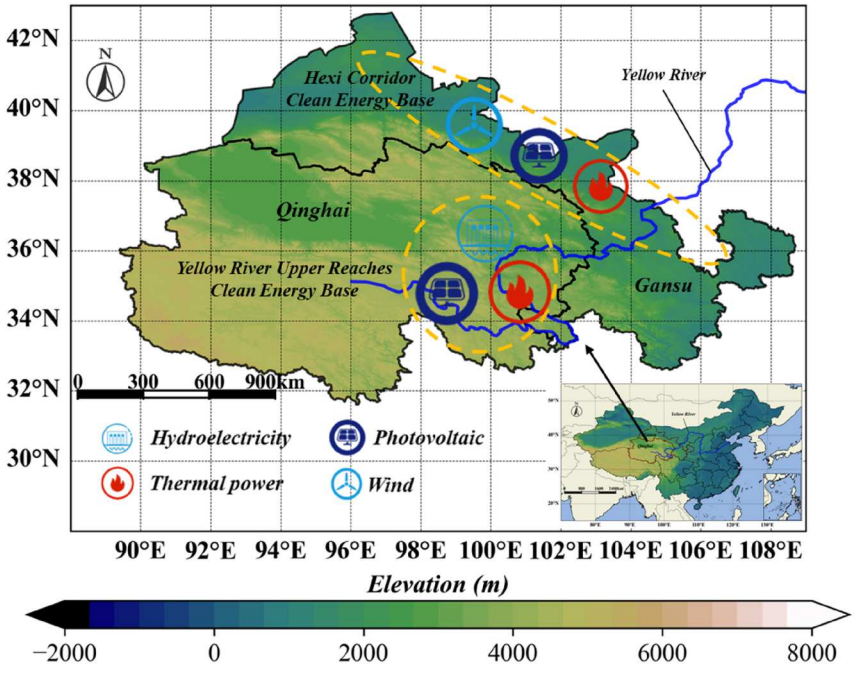

Figure 1. Location of the study area for climate model data fusion.

2.2. Climate model data

Future radiation data were obtained using CMIP6 output data from https://esgfnode.llnl.gov/search/cmip6/ (Juckes et al. 2020). CMIP6 covers 23 sub-programs with 112 model configurations. In this paper, we used 22 CMIP6 models (see Table 1), extracted CMIP6 modelled lunar surface radiation data from CMIP6 models for the period 1979–2014 for SCAF model training, and extracted four shared socioeconomic pathway (SSP) data from CMIP6 GCMs for the period 2015–2099 for future projections. In order to ensure data consistency, the resolution of observed and future climate model data was harmonised.

Figure 2 shows the correlation between radiation historical data and observations (monthly radiation data from 1979–2014) at different time scales for 22 climate models. The results show that most CMIP6 models and the observed data at different time scales show positive correlations, a tiny fraction reaches the significance level of $\alpha = 0.1$. Among them, the GFDL-ESM4 of CMIP6 has a much larger correlation coefficient, and the maximum correlation coefficient is only 0.42 and does not reach the significance level of $\alpha = 0.1$. The RMSE of different models on different time scales also differ significantly, with BCC-CSM2-MR being larger than the other models, exceeding 60 W/m^2, and the smaller CESM2 exceeding 5 W/m^2. The monthly average radiation distributions of the different models differ considerably. In short, different model data in CMIP6 show significant differences in simulating the radiation in the UYRB, and any single model in CMIP6 is not able to describe the radiation distribution of the UYRB well at different time scales. Therefore, it is very necessary to fuse the model data in CMIP6.

Table 1. A summary of the 22 CMIP6 models used in the study.

No.	Model name	Country	Institution	Resolution
1	ACCESS-CM2	Australian	CSIRO, Australian Research Council Centre of Excellence for Climate System Science	144 × 192
2	AWI-CM-1-1-MR	Germany	Alfred Wegener Institute	192 × 384
3	BCC-CSM2-MR	China	Beijing Climate Center	160 × 320
4	CanESM5-CanOE	Canadian	Canadian Centre for Climate Modelling and Analysis	64 × 128
5	CESM2	USA	National Center for Atmospheric Research	192 × 288
6	CMCC-CM2-SR5	Italy	Centro Euro-Mediterraneo sui Cambiamenti Climatici	192 × 288
7	CNRM-CM6-1	France	Centre National de Recherches Météorologiques	128 × 256
8	CNRM-CM6-1-HR	France	Centre National de Recherches Météorologiques	360 × 720
9	CNRM-ESM2-1	France	Centre National de Recherches Météorologiques	128 × 256
10	EC-Earth3-Veg-LR	EC	EC-Earth Consortium	160 × 320
11	FGOALS-f3-L	China	LASG, Institute of Atmospheric Physics, CAS	180 × 288
12	GFDL-ESM4	USA	NOAA Geophysical Fluid Dynamics Laboratory	180 × 288
13	INM-CM4-8	Russia	Institute for Numerical Mathematics	120 × 180
14	INM-CM5-0	Russia	Institute for Numerical Mathematics	120 × 180
15	IPSL-CM6A-LR	France	Institute Pierre-Simon Laplace	143 × 144
16	MIROC6	Japan	Atmosphere and Ocean Research Institute	128 × 256
17	MIROC-ES2L	Japan	Atmosphere and Ocean Research Institute	128 × 256
18	MPI-ESM1-2-LR	Germany	Max Planck Institute for Meteorology	96 × 192
19	MRI-ESM2-0	Japan	Meteorological Research Institute	96 × 192
20	NorESM2-MM	Norway	Norwegian Climate Centre	192 × 288
21	TAIESM1	China	Taiwan Earth System Model Project	192 × 288
22	UKESM1-0-LL	UK	Met Office Hadley Centre	144 × 192

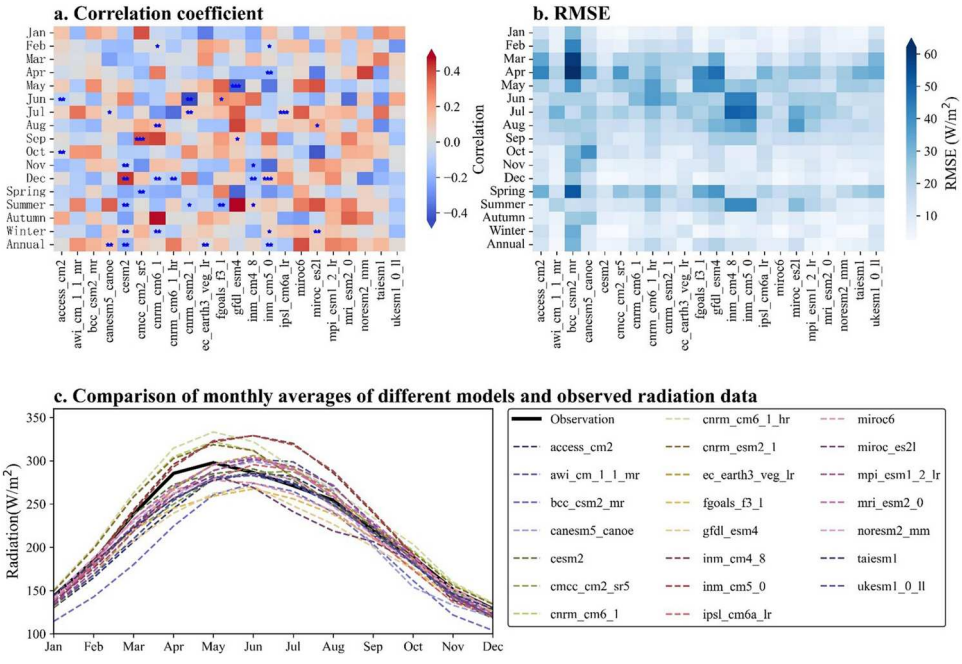

Figure 2. Comparison of radiation data from 22 CMIP6 models (1979–2014) with observations at different time scales. (*, **, ***) indicate significance levels, with * for 0.1, ** for 0.05, and *** for 0.01 significance tests.

2.3. Methods

This study proposes a spatial context-aware fusion (SCAF) model to fuse multi-source climate data by constructing distinct models, not just varied parameters of an identical model, at different spatial locations, as shown in Figure 3. The model fuses data from multiple climate models to capture comprehensive and diverse regional

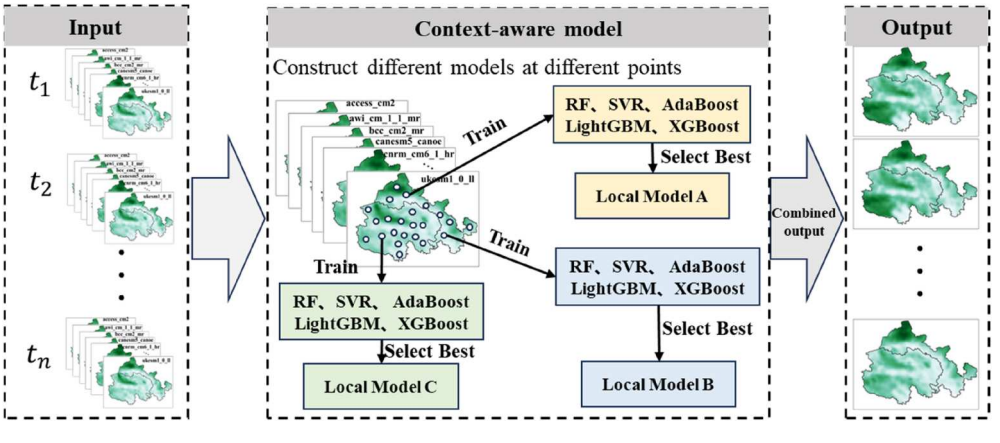

Figure 3. Schematic overview of the spatial context-aware fusion (SCAF) model for fusing multi-source climate data.

climate information. Using the same model with the same parameters or the same model with different parameters in the study area ignores spatial heterogeneity and leads to increased errors in the fused data. Constructing distinct models at different spatial locations effectively addresses the limitations of single model in capturing local features, thereby improving the accuracy and adaptability of climate predictions.

SCAF model contains the following stages. First, the different climate model data at each spatial location and time node are extracted, and five models – Random Forest (RF), Support Vector Regression (SVR), AdaBoost, LightGBM, and XGBoost – are trained for the fusion. Second, the optimal model for each spatial location is selected through the regional comparison of multiple models with five-fold cross-validation. Finally, the above two steps are repeated to achieve the overall fusion of all spatial locations.

3. Results

3.1. Deriving locally optimal models for fusion

Figure 4 shows the model with the optimal performance at each spatial location. For each spatial location, five models, RF, SVR, AdaBoost, LightGBM, and XGBoost, are used, and the optimal model is determined by five-fold cross-validation. When training the model, since the model and parameters at each location are independent of each other, parallel operation is used to train the model at all locations simultaneously to improve the computational efficiency. The results show that the better performing models in the study area are RF, AdaBoost, and LightGBM. SVR and XGBoost perform poorly compared to RF, AdaBoost, and LightGBM. RF performs best in most of the areas.

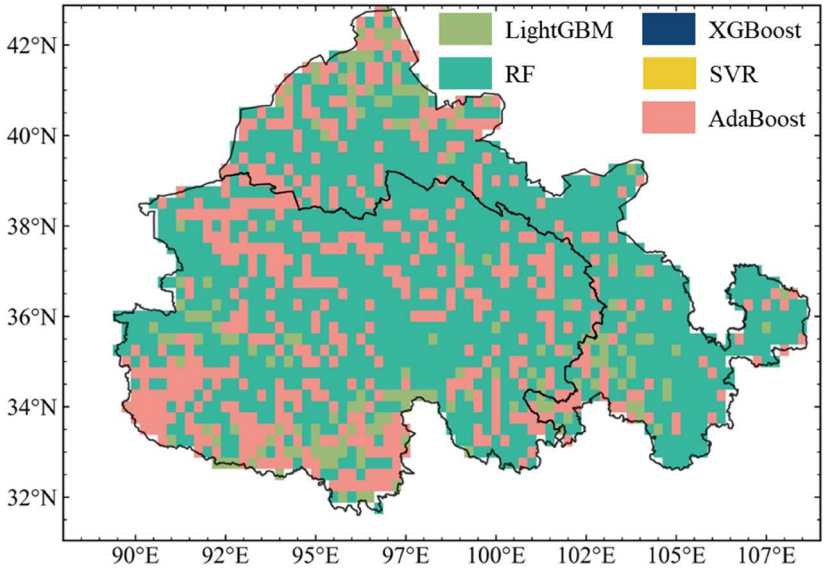

Figure 4. Spatial distribution of the optimal model at each location for climate model data fusion.

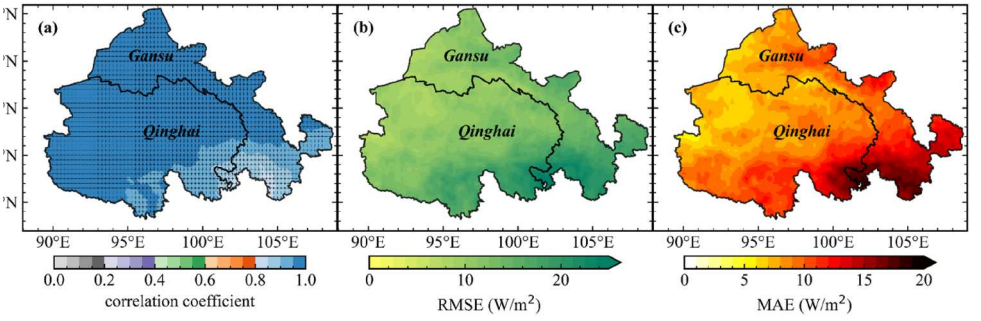

Figure 5. Spatial distributions of evaluation indicators. (a) Correlation coefficient, '+' indicates $p < 0.05$, (b) RMSE, and (c) MAE.

3.2. Model validation

The monthly average radiation data from 1979 to 2009 were set as training data, and the monthly average radiation data from 2010 to 2014 were used for validation. Correlation coefficient (cc), root mean square error (RMSE), and mean absolute error (MAE) were used as model performance evaluation metrics (Meng et al. 2024).

Figure 5 shows the spatial distribution of cc, RMSE, and MAE. The correlation between the fused and observed radiation data is greater than 0.8 for all areas and greater than 0.95 for most areas. The RMSE and MAE in most areas are lower than 12 W/m^2, showing a distribution of high in the southeast and low in the northwest.

Figure 6 shows the spatially averaged comparison of the fused radiation with the observed radiation and the spatially unfolded comparison. The correlation between spatially averaged fused and observed radiation was 0.98 with a RMSE of 7.9. The correlation coefficient was higher than that of any of the climate model data. SCAF was effective in improving the representativeness of the modelled data for the area. Figure 6(c) shows the spatial spread of the 36th and 53rd-month data, and the spatial distributions of the observed and fused radiations are very consistent. The 36th data spread reveals that the fused data in the northwest area underestimates the actual radiation, and the 53rd data spread reveals that the fused data in the southeast area overestimates the actual radiation.

Table 2 summarises the model validation metrics for the linear models, linear weighting models and single machine learning models, and SCAF models, which includes the accuracy improvements of the linear weighting models, single machine learning models SCAF models relative to the linear models. he results show that SCAF models substantially enhance the goodness-of-fit for predictions and significantly reduce prediction errors compared with linear models. Compared to the linear model, the R^2 values for the SCAF model predictions increased by 19.5%, while the RMSE values decreased by 42.8%, and the MAE values decreased by 33.7%. Compared to the single machine learning model, the R^2 values for the SCAF model predictions increased by 5.4%, while the RMSE values decreased by 19.4%, and the MAE values decreased by 23.0%. The SCAF models effectively identify the necessary models for different spatial strata, thereby improving overall prediction accuracy through enhanced local predictive precision.

Overall, the SCAF can fuse the 22 modelled radiation data well and correlates better with the observed data than any single climate model data.

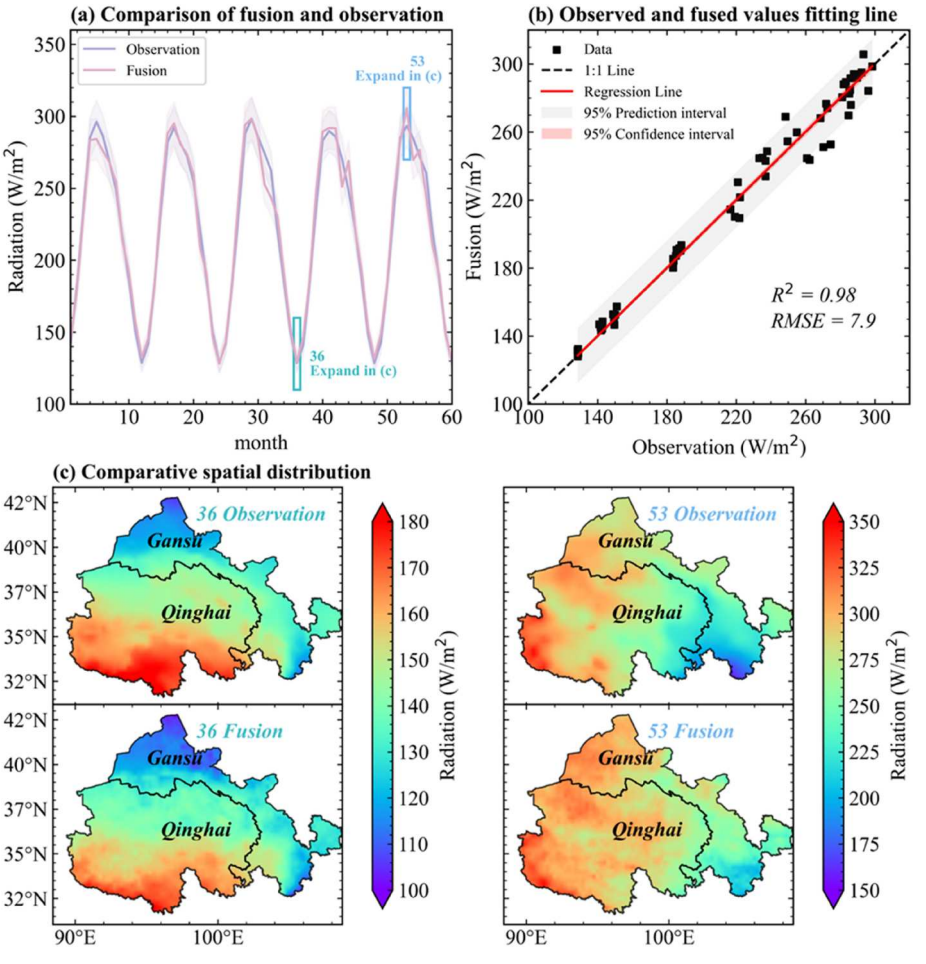

Figure 6. Comparison of fused versus observed radiation (a, b) and comparison of the spatial distribution of fused and observed radiation for 36th and 53rd-month (c).

3.3. Future radiation prediction

3.3.1. Temporal trends in radiation under future climate models

The future radiation changes of the four SSPs show a significant downward trend, which increases with the enhancement of the SSPs (Figure 7).

Table 2. A summary of model validation by comparing SCAF models with the linear models, linear weighting models and single machine learning models.

				Improvements compared to LN		
	cc	RMSE	MAE	cc (%)	RMSE (%)	MAE (%)
LM	0.82	13.8	8.6	–	–	–
LWM	0.90	11.4	7.8	9.8	17.4	9.3
ML	0.93	9.8	7.4	13.4	29.0	14.0
SCAF	0.98	7.9	5.7	19.5	42.8	33.7

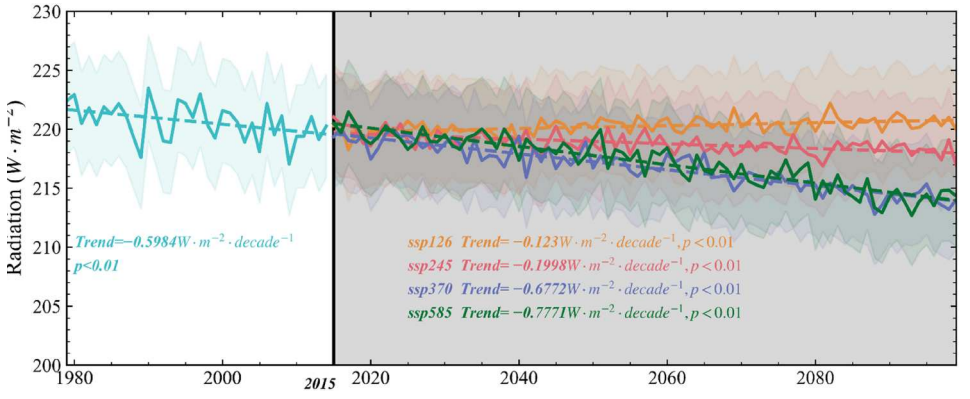

Figure 7. Future trends of the UYRB radiation of the four SSPs.

The seasonal characteristics of the future and current monthly average radiation differences (future minus current) and trends under the four SSPs were analysed in detail (Figure 8). In the near term (2021–2040), the radiation differences in the four seasons show different characteristics. The radiation differences in spring and winter are negative, indicating that future radiation in spring and winter will be lower than current levels. Radiation differences between summer and autumn are positive,

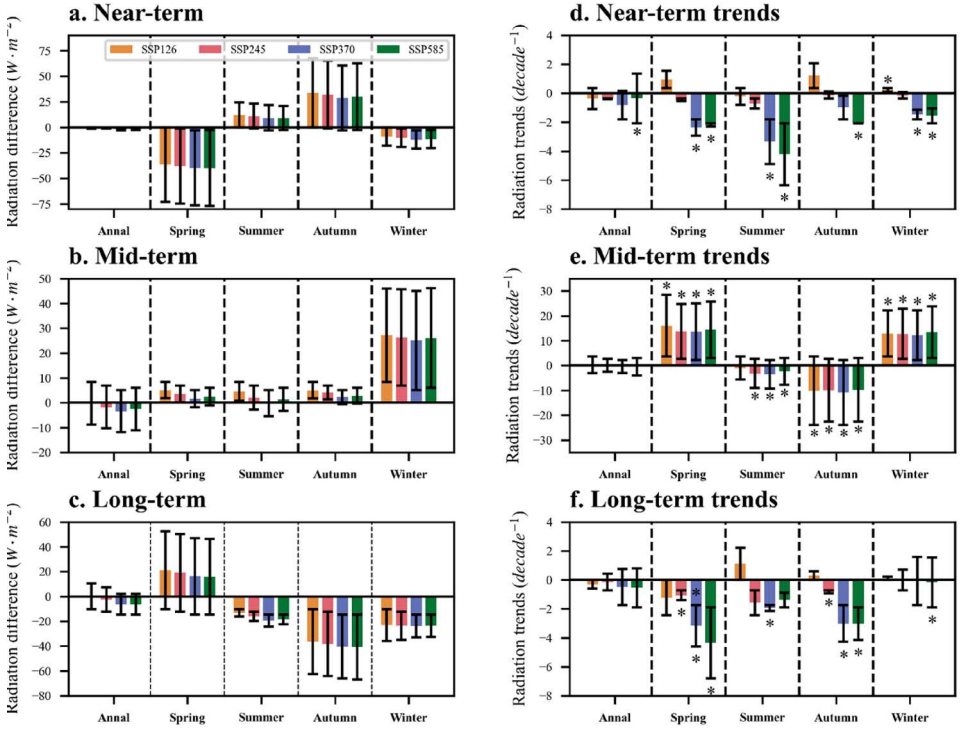

Figure 8. Monthly average radiation differences and trends, * indicates $p < 0.05$.

indicating that future radiation in summer and autumn will be higher than current levels. The difference in radiation between summer and winter is essentially within 10 W/m^2, with small variations, and the difference between spring and autumn is 30 W/m^2, with large variations.

Results for the medium term (2041–2060) show that all scenarios have positive radiation differences for all seasons, indicating that radiation will increase in the future, with the largest difference of 25 W/m^2 in winter, and the rest of the seasons having differences within 10 W/m^2.

The long term (2081–2100) results show positive radiation differences in the spring and negative radiation differences in the remaining three seasons. This suggests that radiation will increase in the spring in the future, while precipitation will increase in the summer, fall, and winter. As the SSP scenario intensifies, the magnitude of the negative difference becomes larger and the magnitude of the positive difference becomes smaller, suggesting that higher SSP scenarios will lead to more significant radiative reductions. However, the effect of forcing scenario intensity on monthly mean radiation is not linear. The difference in monthly average radiation compared to the current climate does not strictly increase (decrease) as the SSP is strengthened (weakened).

In addition to differences in monthly average radiation relative to the current climate, monthly average radiation trends also differ between seasons (Figure 8(d–f)). In the near and long term, monthly average radiation mostly shows a decreasing trend, with the decreasing trend being more significant in the strong scenario than in the weak scenario. The medium-term monthly average radiation shows a significant increasing trend in spring and winter and a significant decreasing trend in summer and autumn.

In general, monthly average radiation is likely to decrease in different future seasons relative to the current climate, and this change is characterised by non-linearity under different scenarios. Although the uncertainty in the radiation differences is smaller than that in the radiation trends, the uncertainty in the projected trends in the medium and long term is higher, and the seasonal characteristics of future radiation changes are complex and varied.

Figure 9 shows the distribution of radiation for each future month under the four SSPs. The future monthly average radiation differs significantly between scenarios and months. The radiation gradually increases from January to a peak in May and then gradually decreases during the summer. This trend is consistent across all SSP scenarios, indicating some regularity in seasonal radiation changes.

Radiation in the SSP126 scenario is generally higher than in the other scenarios and is particularly pronounced in the months of March and April. This suggests that radiation may increase in these months in the future under a lower GHG emissions scenario. Radiation varies less between scenarios in the spring, but is slightly higher in the SSP126 scenario than in the other scenarios, probably because of the low emissions scenario.

The whiskers and anomalies in the boxplots show the range of fluctuations and extremes of radiation for each month. Overall, radiation fluctuates more and has higher uncertainties in the spring months (March through May), especially in April and May, when the scenarios have a wider distribution of radiation. Radiation in the winter and spring months (December to May) is less variable and has lower uncertainties.

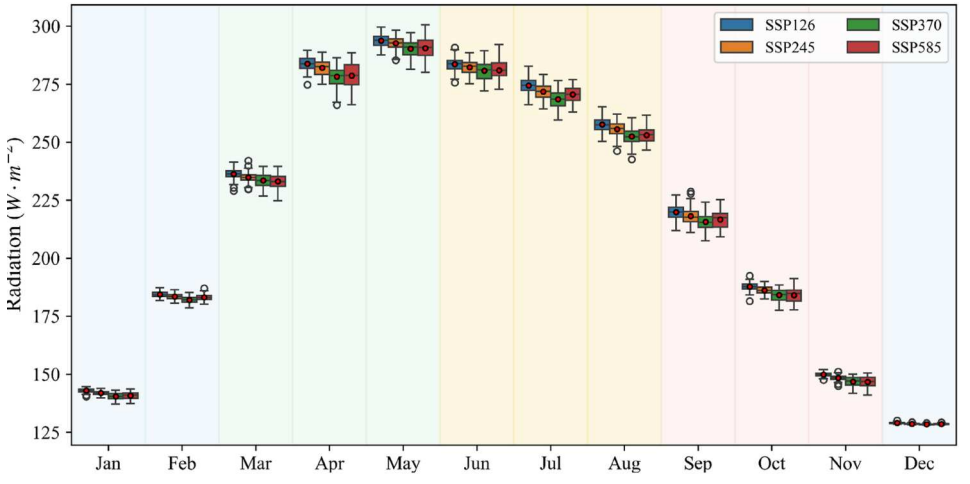

Figure 9. Intra-annual radiation distribution under four future SSPs in the UYRB.

3.3.2. Spatial trends in radiation under future climate models

Figure 10 shows the spatial distributions and trends of monthly average radiation changes in the UYRB for near, medium, and long term under the four SSPs. The spatial distributions and trends of future radiation changes under different SSPs show significant heterogeneity. The higher SSP scenarios (e.g. SSP370 and SSP585) show greater magnitude and uncertainty in the radiation changes and display more complex spatial distribution patterns. the SSP245 scenario shows more moderate radiation changes, while the remaining scenarios show more intense radiation changes.

Figure 11 shows the spatial distribution of changes in monthly average radiation relative to the current climate for the four SSPs. The difference between future radiation and current becomes more and more obvious with increasing time. Qinghai Future radiation is less than current radiation in all four scenarios. In SSP126 and SSP245, the future radiation in Gansu is mostly larger than the current radiation, and only a small part is close to the current radiation. It is noteworthy that at the same SSP, the radiation differences in different periods show similar spatial distributions, suggesting that changes in the SSP did not significantly alter the mean climatic state of radiation. Compared with the radiation trend, the changes in SSP have relatively small effects on the spatial variations of the radiation differences, which suggests that the changes in SSP have greater effects on the radiation trend than on the radiation average.

4. Discussion

This study proposes a spatial context-aware fusion (SCAF) model, which realises adaptive fusion of multi-source climate data by constructing differentiated fusion submodule at different spatial locations. The method fully considers the heterogeneity characteristics between different spatial locations and can effectively improve the applicability of climate data fusion and the robustness of model prediction. SCAF model was applied to the fusion of UYRB radiometric data with more accurate fusion results compared with the

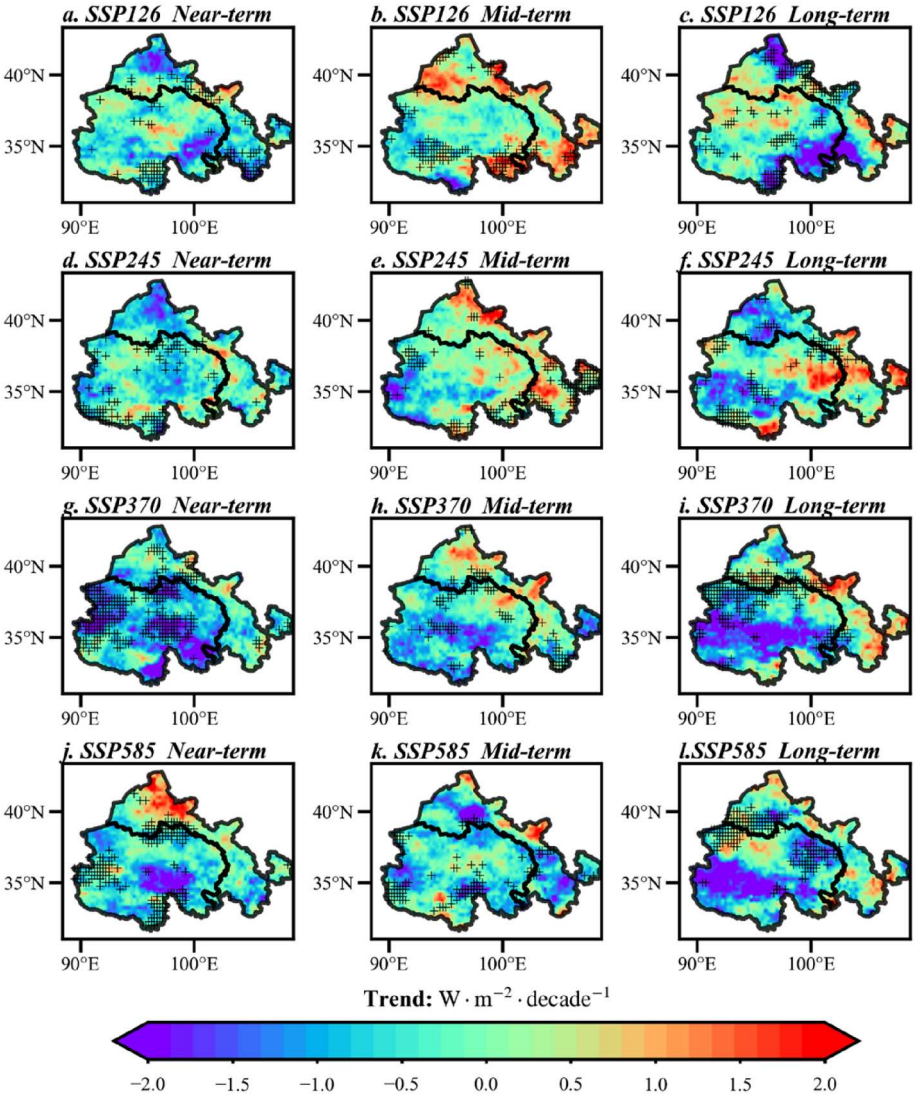

Figure 10. Spatial distributions of near-, medium- and long-term radiation trends under the four SSPs (+ indicates $p < 0.05$).

existing fusion approaches. First, all the time series data of each spatial location under different climate models were extracted, and multiple models were trained at each spatial location, resulting in the best-performing model as the fusion model for that spatial location. Different models were constructed for different spatial locations, effectively capturing the local climate characteristics. Compared with a single fusion model, SCAF greatly improves the overall fusion accuracy. Taking the fusion of radiation data from the UYRB as an example, 22 climate model data were selected as the fusion objects, and the observed data were used as the labels, and RF, XGBoost, AdaBoost, SVR, and LightGBM were chosen as the pre-selected models for the spatial location-by-spatial location model training. The correlation between the SCAF fused radiation

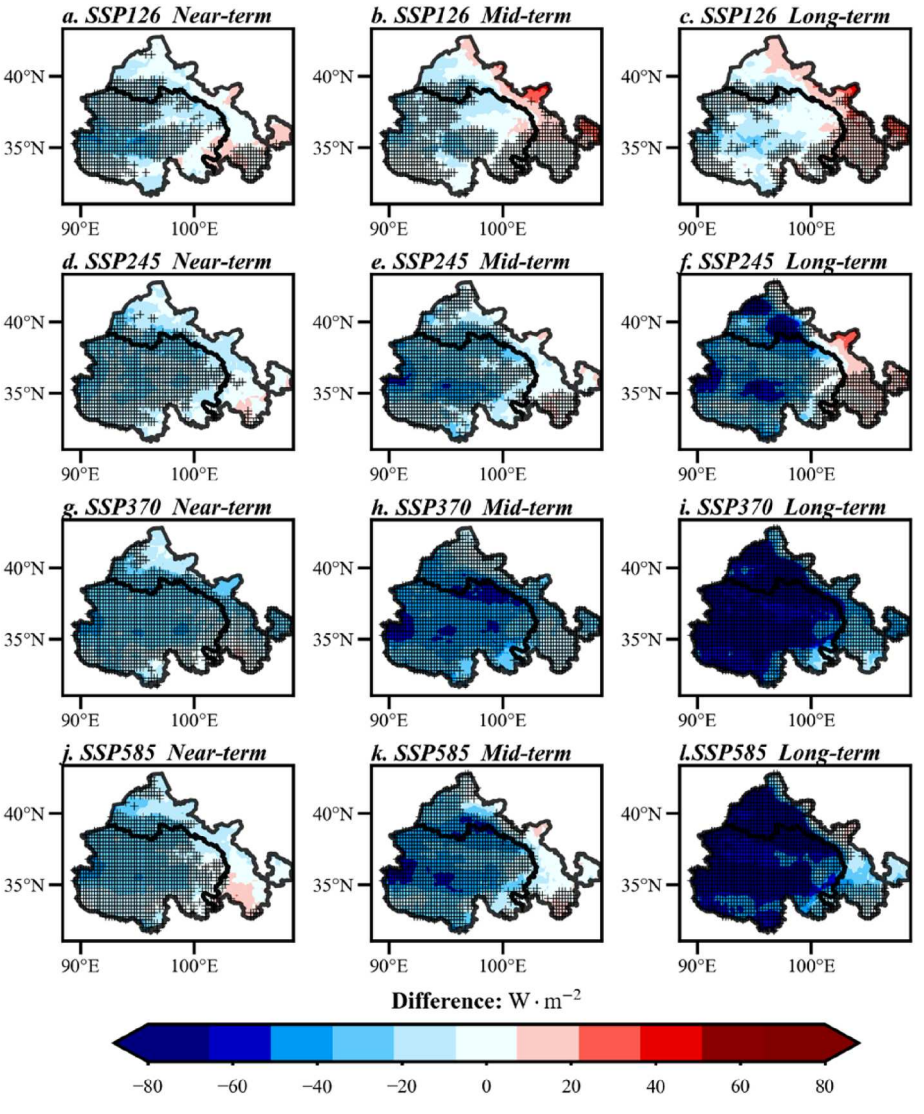

Figure 11. Spatial distributions of radiation differences in the UYRB relative to the current climate (+ indicates $p < 0.05$).

data and the observed data is more than 0.95. Compared to a single machine learning fusion model, the SCAF model demonstrated a significant improvement in overall fusion accuracy, with a correlation coefficient improvement of 5.4%. In addition, SCAF can better reflect the local radiation characteristics than a single model. Finally, the analysis of future radiation changes in the UYRB shows an obvious decreasing trend, and the stronger the scenario model is, the greater the rate of radiation reduction is, with a decreasing rate ranging from 0.123 to 0.7771 W/m^2 per decade.

Based on the results of this study, future research can explore the following aspects in depth. First, SCAF, as a framework model, provides new methods and tools for solving the problem of spatial heterogeneity. In order to further improve the performance of the

fusion model, a wider range of applied research can be carried out by combining multiple algorithms. In addition to the machine learning models used in this study, methods such as neural network models, spatial prediction models, and so on (Panahi et al. 2020) can be introduced to enhance the adaptability and prediction ability of the models. Second, since constructing different models at each spatial location significantly increases the computational cost, such as the amount of computation and time consumed, the development of parallel computing algorithms or spatial stratification in combination with spatial heterogeneity modelling (Guo et al. 2022) can be considered in the future to reduce the model complexity. The SCAF provides an effective data processing method for future climate model research, as well as a new research path for the analysis of regional climate data.

5. Conclusions

Acquiring more accurate climate model data is the basis of regional climate research. This study develops a spatial context-aware model to fuse multi-source climate data by constructing distinct models, not just varied parameters of an identical model, at different spatial locations. SCAF model fuses multiple climate model data by training different models at each spatial location to achieve more accurate and efficient data fusion. In the fusion process of radiation data in the UYRB, SCAF shows excellent results, and its advantages are not only reflected in improving the applicability of climate model data in the area but also in reflecting the local climate characteristics well. In addition, SCAF has great scalability and universality, which provides a new way for the application of climate model data.

Disclosure statement

No potential conflict of interest was reported by the author(s).

Data availability statement

The data that support the findings of this study are available from the corresponding author upon reasonable request.

Reference

Aadhar, S., and V. Mishra. 2020. "On the Projected Decline in Droughts over South Asia in CMIP6 Multimodel Ensemble." *Journal of Geophysical Research: Atmospheres* 125 (20): e2020JD033587. https://doi.org/10.1029/2020JD033587.

Basak, D., N. Garlapati, and J. Patel. 2024. "Identification of Best CMIP6 Climate Models for Offshore Wind Energy Assessment." In *Innovation in Smart and Sustainable Infrastructure: Select Proceeding of ISSI 2022. Lecture Notes in Civil Engineering Vol. 364*, edited by D. Patel, B. Kim, and D. Han, 443–454. Singapore: Springer. https://doi.org/10.1007/978-981-99-3557-4_33.

Basak, D., G. Nagababu, H. Puppala, J. Patel, and S. V. A. Kumar. 2023. "Foreseeing the Spatio-Temporal Offshore Wind Energy Potential of India Using a Differential Weighted Ensemble Created Using CMIP6 Datasets." *Regional Studies in Marine Science* 65:103066. https://doi.org/10.1016/j.rsma.2023.103066.

Chen, Y., N. Wang, J. Jiao, Li, J., Bai, L., Liang, Y., Wei, Y., et al. 2024. "Predicting Soil Loss in Small Watersheds Under Different Emission Scenarios from CMIP6 Using Random Forests." Earth Surface Processes and Landforms 49: 4469–4484. https://doi.org/10.1002/esp.5980.

Deng, X., D. He, G. Zhang, S. Zhu, R. Dai, X. Jin, W. Fu, et al. 2022. "Comparison of Horizontal Wind Observed by Wind Profiler Radars with ERA5 Reanalysis Data in Anhui, China." *Theoretical and Applied Climatology* 150 (3-4): 1745–1760. https://doi.org/10.1007/s00704-022-04247-6.

Deser, C., F. Lehner, K. B. Rodgers, T. Ault, T. L. Delworth, P. N. DiNezio, A. Fiore, et al. 2020. "Insights from Earth System Model Initial-Condition Large Ensembles and Future Prospects." *Nature Climate Change* 10 (4): 277–286. https://doi.org/10.1038/s41558-020-0731-2.

Dey, A., D. P. Sahoo, R. Kumar, and R. Remesan. 2022. "A Multimodel Ensemble Machine Learning Approach for CMIP6 Climate Model Projections in an Indian River Basin." *International Journal of Climatology* 42 (16): 9215–9236. https://doi.org/10.1002/joc.7813.

Dutta, R., K. Chanda, and R. Maity. 2022. "Future of Solar Energy Potential in a Changing Climate across the World: A CMIP6 Multi-model Ensemble Analysis." *Renewable Energy* 188:819–829. https://doi.org/10.1016/j.renene.2022.02.023.

Dutta, U., A. Hazra, H. S. Chaudhari, S. K. Saha, S. Pokhrel, and U. Verma. 2022. "Unraveling the Global Teleconnections of Indian Summer Monsoon Clouds: Expedition from CMIP5 to CMIP6." *Global and Planetary Change* 215:103873. https://doi.org/10.1016/j.gloplacha.2022.103873.

Esnaola, G., A. Ulazia, J. Sáenz, and G. Ibarra-Berastegi. 2024. "Future Changes of Global Annual and Seasonal Wind-Energy Production in CMIP6 Projections considering air Density Variation." *Energy* 307:132706. https://doi.org/10.1016/j.energy.2024.132706.

Ferreira, G. W., M. S. Reboita, and J. G. M. Ribeiro. 2024. "Assessment of the Solar Energy Potential over South America Estimated by CMIP6 Models in the Present and Future Climate." *Journal of Environmental & Earth Sciences* 6 (2): 110–143. https://doi.org/10.30564/jees.v6i2.6425.

Guo, J., J. Wang, C. Xu, and Y. Song. 2022. "Modeling of Spatial Stratified Heterogeneity." *GIScience & Remote Sensing* 59 (1): 1660–1677. https://doi.org/10.1080/15481603.2022.2126375.

Ha, S., Z. Zhou, E. S. Im, and Y. M. Lee. 2023. "Comparative Assessment of Future Solar Power Potential Based on CMIP5 and CMIP6 Multi-model Ensembles." *Renewable Energy* 206:324–335. https://doi.org/10.1016/j.renene.2023.02.039.

Hirsch, A. L., N. N. Ridder, S. E. Perkins-Kirkpatrick, and A. Ukkola. 2021. "CMIP6 MultiModel Evaluation of Present-Day Heatwave Attributes." *Geophysical Research Letters* 48 (22): e2021GL095161. https://doi.org/10.1029/2021GL095161.

Jiang, Y., S. Han, C. Shi, T. Gao, H. Zhen, and X. Liu. 2021. "Evaluation of HRCLDAS and ERA5 Datasets for Near-Surface Wind over Hainan Island and South China sea." *Atmosphere* 12 (6): 766. https://doi.org/10.3390/atmos12060766.

Juckes, M., K. E. Taylor, P. J. Durack, B. Lawrence, M. S. Mizielinski, A. Pamment, J.-Y. Peterschmitt, M. Rixen, and S. Sénési. 2020. "The CMIP6 Data Request (DREQ, Version 01.00.31)." *Geoscientific Model Development* 13 (1): 201–224. https://doi.org/10.5194/gmd-13-201-2020.

Kayhomayoon, Z., M. R. Jamnani, S. Rashidi, S. G. Milan, N. A. Azar, and R. Berndtsson. 2023. "Soft Computing Assessment of Current and Future Groundwater Resources under CMIP6 Scenarios in Northwestern Iran." *Agricultural Water Management* 285:108369. https://doi.org/10.1016/j.agwat.2023.108369.

Li, D., S. Hu, J. Guo, K. Wang, C. Gao, S. Wang, and W. He. 2022. "A New Hybrid Machine Learning Model for Short-Term Climate Prediction by Performing Classification Prediction and Regression Prediction Simultaneously." *Journal of Meteorological Research* 36 (6): 853–865. https://doi.org/10.1007/s13351-022-1214-3.

Martinez, A., and G. Iglesias. 2022. "Climate Change Impacts on Wind Energy Resources in North America Based on the CMIP6 Projections." *Science of the Total Environment* 806:150580. https://doi.org/10.1016/j.scitotenv.2021.150580.

Meng, J., Z. Dong, G. Fu, S. Zhu, Y. Shao, S. Wu, and Z. Li. 2024. "Spatial and Temporal Evolution of Precipitation in the Bahr el Ghazal River Basin, Africa." *Remote Sensing* 16:1638. https://doi.org/10.3390/rs16091638.

Panahi, M., N. Sadhasivam, H. R. Pourghasemi, F. Rezaie, and S. Lee. 2020. "Spatial Prediction of Groundwater Potential Mapping Based on Convolutional Neural Network (CNN) and Support Vector Regression (SVR)." *Journal of Hydrology* 588:125033. https://doi.org/10.1016/j.jhydrol.2020.125033.

Petzold, J., N. Andrews, J. D. Ford, C. Hedemann, and J. C. Postigo. 2020. "Indigenous Knowledge on Climate Change Adaptation: A Global Evidence map of Academic Literature." *Environmental Research Letters* 15 (11): 113007. https://doi.org/10.1088/1748-9326/abb330.

Roshani, A., and M. Hamidi. 2022. "Groundwater Level Fluctuations in Coastal Aquifer: Using Artificial Neural Networks to Predict the Impacts of Climatical CMIP6 Scenarios." *Water Resources Management* 36 (11): 3981–4001. https://doi.org/10.1007/s11269-022-03204-2.

Shuaifeng, S., and Y. Xiaodong. 2022. "Projected Changes and Uncertainty in Cold Surges over Northern China Using the CMIP6 Weighted Multi-model Ensemble." *Atmospheric Research* 278:106334. https://doi.org/10.1016/j.atmosres.2022.106334.

Singh, D., M. Vardhan, R. Sahu, D. Chatterjee, P. Chauhan, and S. Liu. 2023. "Machine-learning- and Deep-Learning-Based Streamflow Prediction in a Hilly Catchment for Future Scenarios Using CMIP6 GCM Data." *Hydrology and Earth System Sciences* 27 (5): 1047–1075. https://doi.org/10.5194/hess-27-1047-2023.

Song, Y., Z. Shen, P. Wu, and R. A. Viscarra Rossel. 2021. "Wavelet Geographically Weighted Regression for Spectroscopic Modelling of Soil Properties." *Scientific Reports* 11:17503. https://doi.org/10.1038/s41598-021-96772-z.

Song, Y., D. Thatcher, Q. Li, T. McHugh, and P. Wu. 2021. "Developing Sustainable Road Infrastructure Performance Indicators Using a Model-Driven Fuzzy Spatial Multi-criteria Decision Making Method." *Renewable and Sustainable Energy Reviews* 138:110538. https://doi.org/10.1016/j.rser.2020.110538.

Song, Y., J. Wang, Y. Ge, and C. Xu. 2020. "An Optimal Parameters-Based Geographical Detector Model Enhances Geographic Characteristics of Explanatory Variables for Spatial Heterogeneity Analysis: Cases with Different Types of Spatial Data." *GIScience & Remote Sensing* 57 (5): 593–610. https://doi.org/10.1080/15481603.2020.1760434.

Tebaldi, C., K. Debeire, V. Eyring, E. Fischer, J. Fyfe, P. Friedlingstein, R. Knutti, et al. 2021. "Climate Model Projections from the Scenario Model Intercomparison Project (ScenarioMIP) of CMIP6." *Earth System Dynamics* 12:253–293. https://doi.org/10.5194/esd-12-253-2021.

Tian, J., Z. Zhang, Z. Ahmed, L. Zhang, B. Su, H. Tao, and T. Jiang. 2021. "Projections of Precipitation over China Based on CMIP6 Models." *Stochastic Environmental Research and Risk Assessment* 35 (4): 831–848. https://doi.org/10.1007/s00477-020-01948-0.

Wang, X., G. Chen, Q. Wu, L. Cao, J. Awange, Y. Song, and M. Wu. 2023. "Spatio-temporal Patterns and Drivers of Carbon–Water Coupling in Frozen Soil Zones across the Gradients of Freezing over the Qinghai-Tibet Plateau." *Journal of Hydrology* 621:129674. https://doi.org/10.1016/j.jhydrol.2023.129674.

Zelinka, M. D., T. A. Myers, D. T. McCoy, S. Po-Chedley, P. M. Caldwell, P. Ceppi, S. A. Klein, and K. E. Taylor. 2020. "Causes of Higher Climate Sensitivity in CMIP6 Models." *Geophysical Research Letters* 47 (1): e2019GL085782. https://doi.org/10.1029/2019GL085782.